

# Enhanced Spin–Orbit Coupled Photoluminescence of Perovskite CsPbBr<sub>3</sub> Quantum Dots by Piezo-Phototronic Effect

Laipan Zhu, Yi-Chi Wang, Ding Li, Longfei Wang, and Zhong Lin Wang\*

Cite This: <https://dx.doi.org/10.1021/acs.nanolett.0c03470>

Read Online

ACCESS |

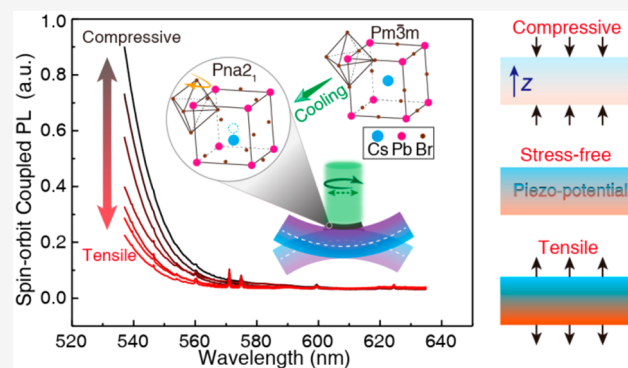
Metrics & More

Article Recommendations

Supporting Information

**ABSTRACT:** Piezo-phototronic effect is a fundamental effect of semiconductors lacking of central symmetry with geometries from one-dimensional (1D) nanowire to 3D bulk. Here, we present that the piezo-phototronic effect can even tune a spin–orbit coupled photoluminescence (PL) based on all-inorganic perovskite CsPbBr<sub>3</sub> quantum dots (QDs). Although the cubic structure of CsPbBr<sub>3</sub> QDs is nonpiezoelectric, a cooling treatment can change it to an orthorhombic structure, which is proven to possess a piezoelectric property. The spin–orbit coupled PL intensity is demonstrated to be dependent on the polarization of the excited light. Because of the manipulation of the spin-split energy levels via the piezo-phototronic effect, the spin–orbit coupled PL intensities under a −0.9% compressive strain for linearly and circularly polarized light excitations can be enhanced by 136% and 146%, respectively. These findings reveal fundamental understandings of the spin–orbit coupled PL dynamics and demonstrate promising optoelectronic applications of the piezo-phototronic effect in these QDs.

**KEYWORDS:** piezo-phototronic effect, piezo-potential, spin–orbit coupling, photoluminescence, all-inorganic perovskites



Halide perovskites have attracted enormous attention due to their excellent optoelectronic properties for applications in solar cells,<sup>1</sup> photodetectors,<sup>2</sup> light-emitting diodes,<sup>3</sup> and lasers.<sup>4</sup> Rapid development in bulk perovskite materials has also inspired extensive researches for perovskite nanostructures. Among them, the all-inorganic colloidal cesium lead halide perovskites (CsPbX<sub>3</sub>, X = Cl, Br, I) quantum dots (QDs) featuring large quantum-size effect have drawn growing interest for their outstanding optical characteristics, which make CsPbX<sub>3</sub> QDs better candidates for new-generation light sources, display techniques, and bioluminescence labeling.<sup>5–8</sup> The discovery and study of the piezoelectric property of inorganic CsPbX<sub>3</sub> QDs are of great significance for high-performance optoelectronic devices. It has been demonstrated that organic–inorganic lead halide perovskites have revealed strong piezoelectricity due to the alignment of organic molecular (such as methylammonium (MA)) dipoles.<sup>9–11</sup> However, in all-inorganic CsPbX<sub>3</sub> QDs the piezoelectric property has been rarely reported. The reason lies in that the CsPbX<sub>3</sub> QDs are usually cubic structure at room temperature, which is a steady structure and hence insensitive to mechanical stimuli.

Piezotronic and piezo-phototronic effects are two born features of semiconductors that lack center symmetry, which have been widely utilized in materials such as third-generation semiconductors, transition-metal dichalcogenides, and organic–inorganic lead halide perovskites to enhance the perform-

ances of electronic and optoelectronic devices.<sup>12–16</sup> The piezo-phototronic effect regards to the regulation of generation, separation, transfer, and/or recombination of electron–hole pairs at semiconductor interfaces by employing strain-induced piezo-potential or piezo-charges. The piezo-phototronic effect has demonstrated a promising way in enhancing the performances of various optoelectronic devices, such as photovoltaic cells,<sup>17,18</sup> light-emitting diodes (LEDs),<sup>19,20</sup> photodetectors,<sup>21,22</sup> and spin devices.<sup>9,23,24</sup>

In this work, the presence of a strong spin–orbit coupling (SOC) in the CsPbBr<sub>3</sub> QDs was confirmed. A strong piezoelectric property in CsPbBr<sub>3</sub> QDs was discovered and investigated after the QDs have undergone a cooling-treated process, which has a great influence on the spin–orbit coupled photoluminescence (PL). The piezo-phototronic effect was used to tune the spin–orbit coupled PL intensity with a simple application of bending strain on the QDs' covered flexible substrate. These findings are of great significance to the development of advanced optoelectronic and spintronic

Received: August 27, 2020

Revised: October 6, 2020

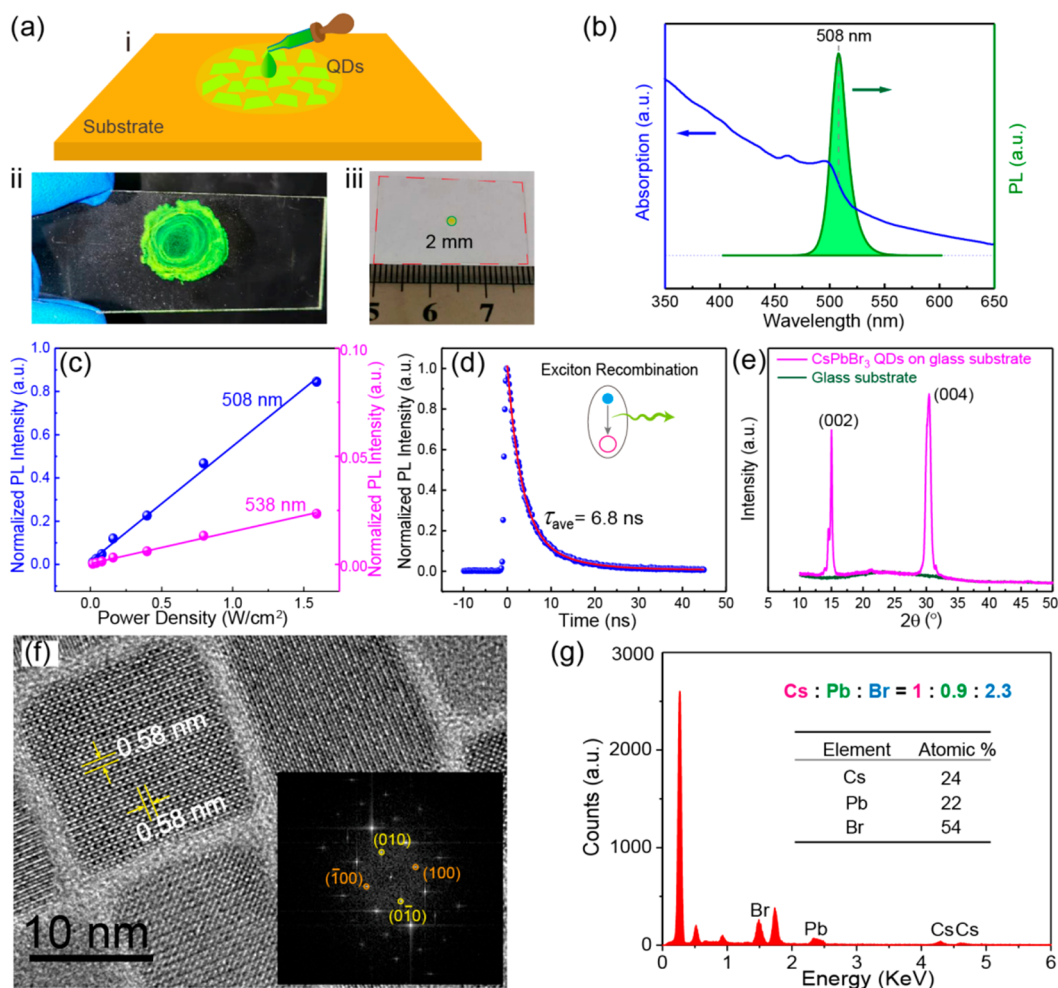


**Figure 1.** Characterization of the all-inorganic perovskite CsPbBr<sub>3</sub> QDs. (a) A schematic diagram of QDs on a substrate (i), an optical image of QDs on a glass substrate (ii), and an optical image of a 2 mm size dropped QDs on PET substrate (iii). (b) Absorption and PL spectra of the QDs. (c) Normalized PL intensity as a function of the power density of a 325 nm laser. (d) TRPL spectrum of the QDs corresponding to 508 nm. (e) XRD of the glass substrate and the QDs/glass. (f) HRTEM image of the CsPbBr<sub>3</sub> QDs along [001] zone axis (z-axis). The inset at the bottom right corner denotes the corresponding FFT image. (g) EDX spectrum of the CsPbBr<sub>3</sub> QDs.

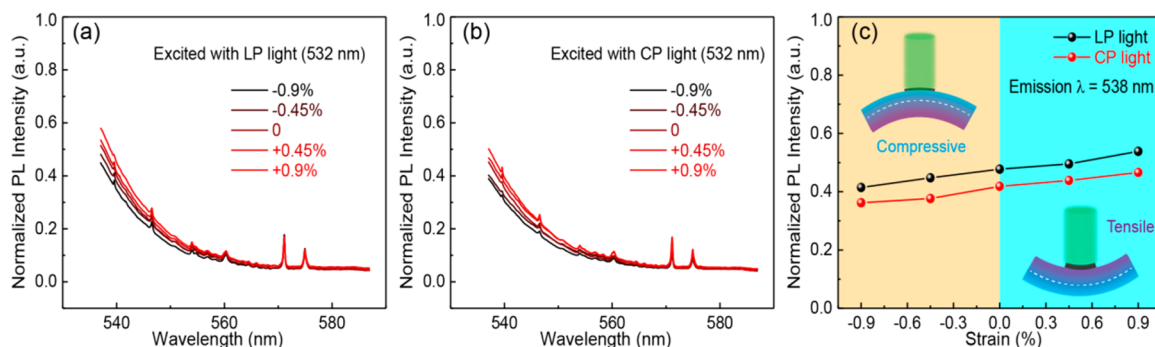


**Figure 2.** Normalized PL spectra of the as-fabricated QDs under different strains. (a,b) Normalized PL spectra excited with LP (a) and CP (b) lights. (c) Normalized PL intensity corresponding to the emission wavelength of 538 nm as a function of strain. The upper left and bottom right insets in (c) sketch the compressive and tensile strains, respectively, along z-axis of the QDs.

applications based on perovskite QDs with outstanding quantum confinement effects.

The CsPbBr<sub>3</sub> QDs' solution showed a light green color (Figure 1a) and was dropped on the surface of a flexible polyethylene terephthalate (PET) substrate with 500  $\mu\text{m}$  in thickness for further applying strain on the QDs (Figure 1a, Figure S1 and Note S1, Supporting Information). Figure 1b

illustrates the absorption and PL spectra of the CsPbBr<sub>3</sub> QDs at 300 K with an optical PL peak of 508 nm and a narrow full width at half-maximum (FWHM) of 17 nm. The diameter of the laser spot for all of the following measurements was 2 mm. The power density dependence of the normalized PL intensity is almost linear for both 508 and 538 nm wavelengths (Figure 1c and Figure S2, Supporting Information). The time-resolved

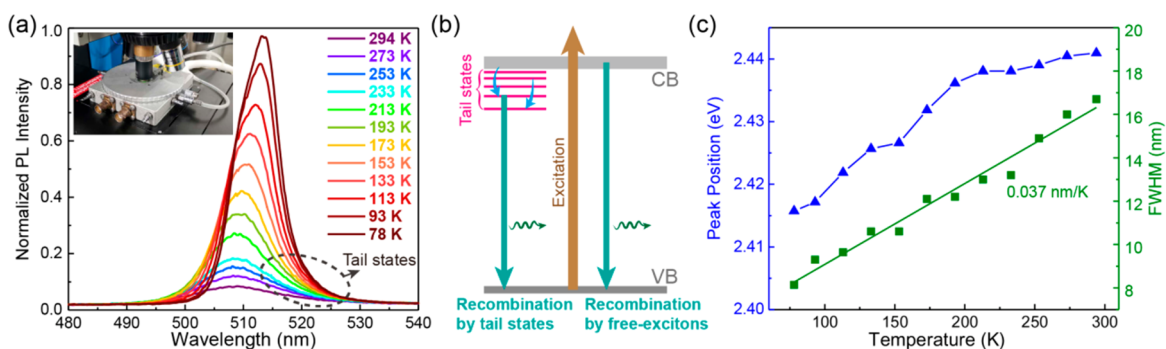


**Figure 3.** Temperature dependence of PL characteristics of CsPbBr<sub>3</sub> perovskite QDs on a p-Si substrate. (a) Normalized PL spectra measured at different temperatures ranging from 78 to 294 K, where the inset denotes an optical image of the cryogenic system combined with laser and microscope for the measurements. (b) Schematic recombination dynamics after a light excitation, where the tail states are sketched below the CB. (c) Peak positions and FWHM of PL spectra under different temperatures extracted from (a).

PL (TRPL) spectrum reveals a fast recombination time of 6.8 ns on average (Figure 1d), indicating that the radiation of CsPbBr<sub>3</sub> QDs is mainly derived from exciton recombination. From the X-ray powder diffraction (XRD), only (002) and (004) indices of the crystal face were detected, which shows a uniform distribution of the CsPbBr<sub>3</sub> QDs with [001] or [00 $\bar{1}$ ] direction (i.e., z-axis) pointing away from the surface of the substrate. The high-resolution transmission electron microscopy (HRTEM) and the corresponding fast Fourier transformation (FFT) images of CsPbBr<sub>3</sub> perovskite QDs (Figure 1f, Figure S3 and Note S2, Supporting Information) indicate a cubic structure of the as-fabricated QDs with a lattice constant of 0.58 nm. Energy dispersive X-ray (EDX) spectrum of the CsPbBr<sub>3</sub> QDs (Figure 1g) reveals the presence of Cs, Pb, and Br elements with the corresponding atomic ratio of 1:0.9:2.3, close to the stoichiometric ratio of 1:1:3. The deviated experimental atomic ratio of QDs from the stoichiometric ratio is probably due to the evaporation of Pb and Br under high-energy TEM electron beam and the limit accuracy of EDX quantification.

The as-fabricated QDs (without cooling treatment) under different strains were excited with linearly polarized (LP) and circularly polarized (CP) 532 nm lasers and the excited PL intensity are shown in Figure 2. The excitation laser was changed to 532 nm so the laser polarization can be tuned via a quarter waveplate working between 400 to 700 nm. The PL intensities excited with LP and CP lights are both increased with the strain varying from  $-0.9\%$  compressive strain to  $+0.9\%$  tensile strain (Figure 2a,b), and the calculation of strain is shown in Note S3 of Supporting Information. Compared with the micrometer-scale thickness of the PET substrate, the nanometer-scale thickness of QDs can be neglected. The QDs are believed to attach to the surface of the PET with a van der Waals force. Hence the bending strain applied on the QDs is approximately equivalent to the strain applied on the upper surface of the PET substrate (insets in Figure 2c). An upward bending (the upper left inset in Figure 2c) of PET brings an in-plane tensile strain and an out-of-plane (i.e., z-axis) compressive strain on the QDs. On the contrary, a downward bending (the bottom right inset in Figure 2c) makes an in-plane compressive strain and an out-of-plane tensile strain. Plotting normalized PL intensities emitted from 538 nm wavelength as a function of strains, Figure 2c shows the normalized PL intensity increases almost linearly with the strain changing from  $-0.9\%$  to  $+0.9\%$ . Such linear correspondence can be attributed to the stronger scattering

of PL light when a compressive strain was applied, while the stronger gathering of PL light can be noted when a tensile strain was applied. That is, the slight change in PL intensity results from different light scatterings with the change of device geometry under different strains. The slightly smaller PL intensity for CP light excitation compared with that of LP light excitation is believed to be derived from the presence of Rashba SOC, and the PL measured in this work will be refined as the spin-orbit coupled PL, whose detailed physical picture will be discussed later.

The temperature dependence of the normalized PL spectra of the CsPbBr<sub>3</sub> perovskite QDs on a p-Si substrate is displayed in Figure 3. The experimental setup is shown in the inset of Figure 3a. When decreasing temperature from 294 to 78 K, the peak intensity of PL spectra is increasing while the PL peak position appears as a reduced photon energy (i.e., a redshift) (Figure 3a). The redshift is opposite to that expected for typical semiconductors such as Si, Ge, and GaAs.<sup>25</sup> The PL spectra are not strictly symmetrical around their peaks, which is believed to be due to the presence of free-exciton and bright tail states that allow different radiative recombinations of excitons localized in the states.<sup>26,27</sup> A diagram of carrier recombination dynamics after electrons excited from the valence band (VB) to the conduction band (CB) is illustrated in Figure 3b. The redshift of the lower-energy peak corresponds to the enhanced recombination of carriers relaxed in the tail states with the decrease of temperature. The temperature dependence of PL peak positions (i.e., photon energies) and that of PL spectra FWHM is summarized in the blue and green labels in Figure 3c, respectively. The recombination luminescence from the bright tail states is becoming much more dominant than that from the free-exciton states with a further decrease of temperature from 200 K; as a result, the peak position shows a severe redshift below 200 K. The PL spectra FWHM shows a linear decrease with a slope of 0.037 nm/K as temperature is decreasing in the whole measured range. In comparison with traditional QDs based on Cd-chalcogenides and rare-earth phosphors, the perovskite QDs possess outstanding quantum efficiency and narrower FWHM of PL intensity spectra. Therefore, perovskite QDs can be synthesized for more saturated colors and hold better application potentials in QLED displays.<sup>6,28,29</sup>

The more interesting phenomenon is that the perovskite CsPbBr<sub>3</sub> QDs demonstrated a piezoelectric property when they experienced a cooling treatment at 200 K for 20 min, and the piezoelectric property can be maintained even when the

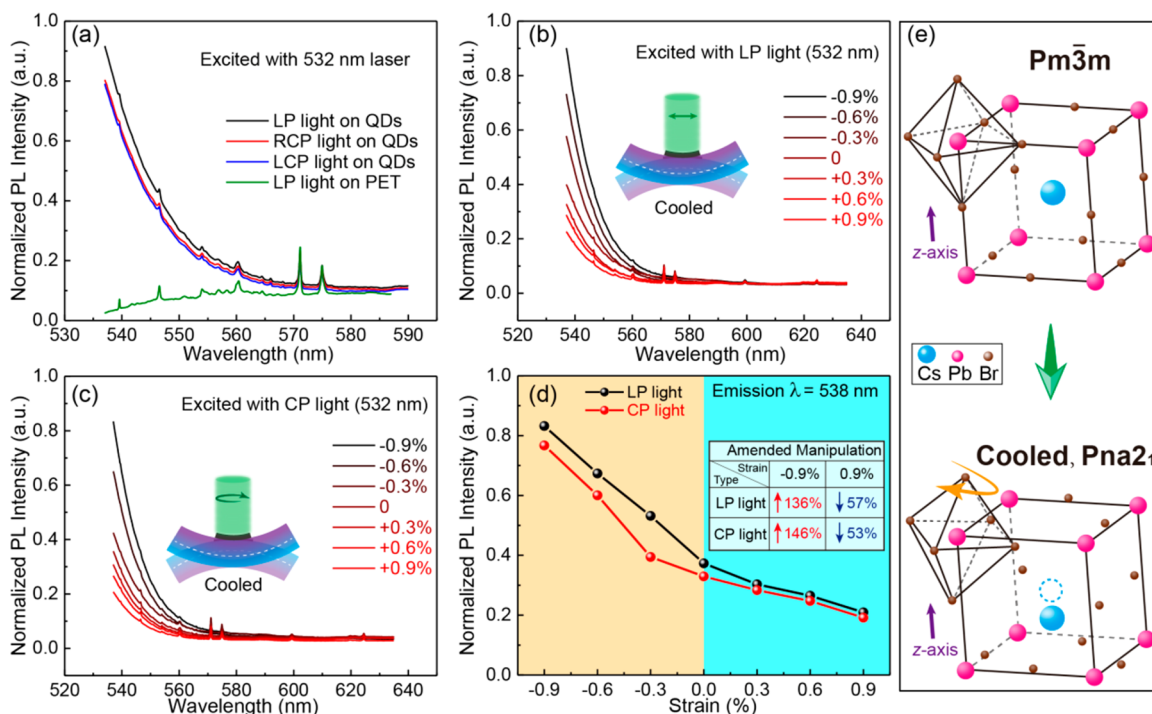


**Figure 4.** Normalized spin–orbit coupled PL of the CsPbBr<sub>3</sub> perovskite QDs after a cooling treatment. (a) Normalized PL spectra of the QDs and PET for different light polarizations. (b) Normalized PL spectra excited with LP light and under different strains. (c) Normalized PL spectra excited with CP light and under different strains. (d) Normalized PL intensity corresponding to the emission wavelength of 538 nm as a function of strain for LP and CP excitations. The inset table illustrates amended manipulations for LP and CP excitations under  $-0.9\%$  and  $0.9\%$  strains. (e) Schematic transformation of phase structure after a cooling treatment of 200 K.

temperature has risen to 292 K (a controlled room temperature). Considering that the low-temperature resistance of the PET substrate is limited to around 200 K, the cooling temperature was thus selected to be 200 K to allow phase transition and not damage the PET substrate. The PL intensity also reveals a dependence on the polarization of the exciting laser light (532 nm). As shown in Figure 4a, the normalized intensity of spin–orbit coupled PL spectrum of the CsPbBr<sub>3</sub> perovskite QDs for both right circularly polarized (RCP) and left circularly polarized (LCP) light excitations are almost the same (Figure 4a red and blue lines, respectively) while slightly smaller than that for LP light excitation (Figure 4a black line). The downward bending of PL for the case of LP light on PET is due to the absorption of PET. Later, the strain dependences of the normalized intensity of the spin–orbit coupled PL spectrum for LP (Figure 4b) and CP (Figure 4c) light excitations were studied. Both investigations reveal PL intensity increases when applied compressive strain increases and decreases when applied tensile strain increases. The normalized spin–orbit coupled PL intensity as a function of strain corresponding to the emission wavelength of 538 nm is extracted in Figure 4d. Note that the manipulations of spin–orbit coupled PL intensity in the table of Figure 4d are amended in consideration of the modulation of PL due to the different light scatterings with the change of device geometry according to Figure 2c. For an LP light excitation, the normalized spin–orbit coupled PL intensity is enhanced by 136% and decreased by 57% under a  $-0.9\%$  compressive strain and a  $0.9\%$  tensile strain, respectively. For a CP light excitation under the same compressive and tensile strain, the spin–orbit coupled PL intensity is enhanced by 146% and decreased by 53%. Compared to untreated QDs (Figure 2c), the PL

intensity response to strains is quite different when QDs have undergone a cooling treatment (Figure 4d and Figure S4, Supporting Information). This is a strong demonstration of the piezo-phototronic effect tuned-photoluminescence based on CsPbBr<sub>3</sub> QDs. The effect should be attributed to the structural transformation of QDs from a cubic structure with a space group of *Pm* $\bar{3}$ *m* to an orthorhombic structure with a space group of *Pna*2<sub>1</sub> due to the cooling treatment, as illustrated in Figure 4e, and the *Pna*2<sub>1</sub> phase can be maintained even at 292 K. But a heating treatment at 310 K for 20 min can turn the *Pna*2<sub>1</sub> phase back to the cubic phase, as demonstrated in Figure S5 (see Supporting Information). The *Pna*2<sub>1</sub> group is a noncentrosymmetric structure, which results in the piezoelectricity of materials.<sup>30,31</sup> Very recently, Li et al. proved that the ferroelectricity in cooling-treated perovskite CsPbBr<sub>3</sub> QDs is due to the distorted structure with twisting and tilting of the [PbBr<sub>6</sub>]<sup>4-</sup> and the off-centered Cs<sup>+</sup> causing a weak separation of centers of positive and negative charges, which were obtained by a polarization-electric field hysteresis loop measurement using a ferroelectric tester.<sup>32</sup> The present work is more evidence of the presence of piezoelectric property for cooling-treated perovskite CsPbBr<sub>3</sub> QDs.

The possible mechanism accounting for the polarization dependence of the spin–orbit coupled PL is proposed. Regarding the CsPbBr<sub>3</sub> QD as a supermolecule, electrons (holes) will move around the supermolecule, whose spins will couple, identically as the single molecule case with the p-orbitals of the Pb (the s-orbital of the Pb and p-orbitals of the surrounding Br), resulting in spin-splittings in the CB and VB with the same spin states of  $|\frac{1}{2}, -\frac{1}{2}\rangle$  and  $|\frac{1}{2}, +\frac{1}{2}\rangle$ .<sup>33–35</sup> The stress-free case shows a spontaneous polarization<sup>32</sup> with a moderate piezo-potential as CsPbBr<sub>3</sub> QDs uniformly oriented

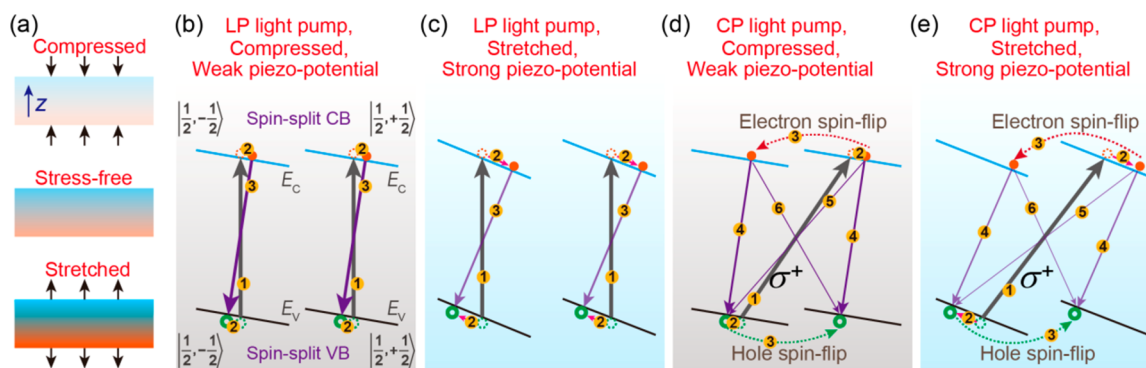


**Figure 5.** Proposed mechanisms of the piezo-phototronic effect tuned spin-orbit coupled PL intensity. (a) Schematic intensity of piezo-potential distribution in  $z$ -axis under compressed, stress-free, and stretched states. Brown and blue colors are, respectively, positive and negative piezo-potentials, where the darker the color is, the stronger the piezo-potential is. (b,c) Schematic radiation recombination processes of electron-hole pairs excited with LP light in spin-split CB and VB under weak (b) and strong (c) piezo-potential. (d,e) Schematic radiation recombination processes of electron-hole pairs excited with CP light in spin-split CB and VB under weak (d) and strong (e) piezo-potential. Labeled numbers with a yellow circle background indicate each process step.

along  $+z$  or  $-z$  axis on the PET substrate. Although the polarity directions of the QDs may be reversed, that is, along  $+z$  or  $-z$ , the variation tendencies of the piezo-potential are the same, that is, both increasing or both decreasing under the same strain. The piezo-potential decreases when QDs are compressed along the  $z$ -axis and increases when QDs are stretched, as illustrated in Figure 5a. An increase of piezo-potential can not only strengthen the Rashba SOC but also severely incline the spin-split band levels. When QDs are excited by an LP light with angular momentum of 0 and compressed with a weaker piezo-potential (i.e., applying a small compressive strain), photoinduced carriers are excited from the spin-split VB ( $|\frac{1}{2}, -\frac{1}{2}\rangle$  and  $|\frac{1}{2}, +\frac{1}{2}\rangle$ ) to the spin-split CB ( $|\frac{1}{2}, -\frac{1}{2}\rangle$  and  $|\frac{1}{2}, +\frac{1}{2}\rangle$ ), respectively, and the carriers will get recombination luminescence between subbands with the same spin angular momentum after suffering a slight drift under the weaker piezo-potential (process 3 in Figure 5b). However, if the piezo-potential is stronger under a tensile strain (stretched case), the electrons and holes with the same spin angular momentum will be separated rapidly (process 2 in Figure 5c), which is relatively difficult for the recombination luminescence (process 3 in Figure 5c). In other words, an increased compressive strain makes an enhanced spin-orbit coupled PL intensity while an increased tensile strain makes a decreased spin-orbit coupled PL intensity for LP light excitation, as shown in Figure 4b,d. As illustrated in Figure 5d, when a CP light, such as a left ( $\sigma^+$ )-handed CP light, is excited on the QDs with a weaker piezo-potential, electrons will be excited from the spin-split VB  $|\frac{1}{2}, -\frac{1}{2}\rangle$  to the spin-split CB  $|\frac{1}{2}, +\frac{1}{2}\rangle$  (process 1 in Figure 5d) according to the optical transition selection rule.<sup>36</sup> The excited spin-polarized electrons and holes will be drifted slightly under the weak piezo-potential (process 2 in Figure 5d) and also experience a spin-flipping to the opposite spin-subband levels nearby (process 3 in Figure 5d); finally a spin-orbit coupled PL intensity is measured due to the carrier recombination corresponding to processes 4, 5, and 6 in Figure 5d. The processes 3 and 4 may be much more dominant than the processes 5 and 6, thus a nearly direct recombination transition of process 4 will emit a large amount of LP light, which is the reason why PL intensity for a CP light

excitation is only slightly reduced compared to that for an LP light excitation (Figure 4a). When a strong piezo-potential is emerged (i.e., a stretched case, see Figure 5e), the spin-split energy levels will be tilted more seriously, and hence the electron-hole pairs will be separated more seriously, which will suppress the recombination luminescence due to the stronger indirect bandgap property. In other words, for a CP light excitation an increased compressive strain will reduce the magnitude of piezo-potential and thus enhance PL intensity, while an increased tensile strain reduces PL intensity, as shown in Figure 4c,d. As they are more severe with indirect recombination for CP light excitation, in general the spin-orbit coupled PL intensity for CP light excitation is weaker compared with that for LP light excitation. Also, the cubic-structured CsPbBr<sub>3</sub> QDs also reveal a Rashba SOC although it does not possess a piezoelectricity (Figure 2c). The PL spectra for RCP and LCP light excitations under the same piezo-potential are nearly the same (Figure 4a) which is probably because the spin-flipping process 3 and the subsequent recombination luminescence process 4 are dominant, whereas the recombination luminescence processes 5 and 6 are relatively weak.

In conclusion, the piezo-phototronic effect is shown to effectively tune the spin-orbit coupled PL intensity based on all-inorganic perovskite CsPbBr<sub>3</sub> QDs. The QDs with a cooling treatment are demonstrated to yield a piezoelectric property and a spontaneous polarization, which can be maintained even after the temperature is raised to 292 K. The piezo-potential can tune not only the Rashba SOC but also the inclination of the spin-split band levels. For LP and CP light excitations, the normalized spin-orbit coupled PL intensities can be enhanced effectively by 136% and 146%, respectively. The spin-orbit coupled PL intensity for LP light excitation is larger than that for CP light excitation due to the different carrier recombination processes in the spin-split band levels. These findings demonstrate that the piezo-phototronic effect can still work at all-inorganic perovskite-based QDs, revealing great potential of advanced optoelectronic and spintronic applications of the piezo-phototronic effect in these QDs.

## ■ ASSOCIATED CONTENT

### SI Supporting Information

The Supporting Information is available free of charge at <https://pubs.acs.org/doi/10.1021/acs.nanolett.0c03470>.

Photograph of PET substrate covered by a circular Kapton tape (Figure S1), normalized PL spectra under different light power (Figure S2), an enlarged view of the HRTEM image (Figure S3), a comparison of the normalized spin–orbit coupled PL intensity for different cooling treatments and light polarizations (Figure S4), normalized spin–orbit coupled PL spectra after a heating treatment (Figure S5), schematic experimental setup and optical path of the measurement (Figure S6), and several notes about experimental methods (Note S1), thickness statement (Note S2), strain calculation (Note S3), piezo-phototronic effect on PL spectrum and the heating effect on piezo-charges (Note S4) (PDF)

## ■ AUTHOR INFORMATION

### Corresponding Author

**Zhong Lin Wang** – CAS Center for Excellence in Nanoscience, Beijing Key Laboratory of Micro-nano Energy and Sensor, Beijing Institute of Nanoenergy and Nanosystems, Chinese Academy of Sciences, Beijing 100083, P.R. China; School of Material Science and Engineering, Georgia Institute of Technology, Atlanta, Georgia 30332, United States; [orcid.org/0000-0002-5530-0380](https://orcid.org/0000-0002-5530-0380); Email: [zhong.wang@mse.gatech.edu](mailto:zhong.wang@mse.gatech.edu)

### Authors

**Laipan Zhu** – CAS Center for Excellence in Nanoscience, Beijing Key Laboratory of Micro-nano Energy and Sensor, Beijing Institute of Nanoenergy and Nanosystems, Chinese Academy of Sciences, Beijing 100083, P.R. China; School of Nanoscience and Technology, University of Chinese Academy of Sciences, Beijing 100049, P.R. China; [orcid.org/0000-0001-7538-641X](https://orcid.org/0000-0001-7538-641X)

**Yi-Chi Wang** – CAS Center for Excellence in Nanoscience, Beijing Key Laboratory of Micro-nano Energy and Sensor, Beijing Institute of Nanoenergy and Nanosystems, Chinese Academy of Sciences, Beijing 100083, P.R. China; School of Nanoscience and Technology, University of Chinese Academy of Sciences, Beijing 100049, P.R. China

**Ding Li** – CAS Center for Excellence in Nanoscience, Beijing Key Laboratory of Micro-nano Energy and Sensor, Beijing Institute of Nanoenergy and Nanosystems, Chinese Academy of Sciences, Beijing 100083, P.R. China; School of Nanoscience and Technology, University of Chinese Academy of Sciences, Beijing 100049, P.R. China

**Longfei Wang** – CAS Center for Excellence in Nanoscience, Beijing Key Laboratory of Micro-nano Energy and Sensor, Beijing Institute of Nanoenergy and Nanosystems, Chinese Academy of Sciences, Beijing 100083, P.R. China; School of Nanoscience and Technology, University of Chinese Academy of Sciences, Beijing 100049, P.R. China; School of Material Science and Engineering, Georgia Institute of Technology, Atlanta, Georgia 30332, United States

Complete contact information is available at: <https://pubs.acs.org/doi/10.1021/acs.nanolett.0c03470>

### Author Contributions

L.Z. and Z.L.W. designed the experiments. L.Z. conducted the experiments. L.Z. and Z.L.W. wrote the manuscript. All coauthors read and commented on the manuscript.

### Notes

The authors declare no competing financial interest.

## ■ ACKNOWLEDGMENTS

This research was supported by the National Natural Science Foundation of China (Grants 11704032, 51432005), the National Key R & D Project from Minister of Science and Technology (2016YFA0202704), the Beijing Municipal Science & Technology Commission (Z171100000317001, Z171100002017017, Y3993113DF).

## ■ REFERENCES

- (1) Zuo, C.; Bolink, H. J.; Han, H.; Huang, J.; Cahen, D.; Ding, L. Advances in perovskite solar cells. *Adv. Sci.* **2016**, *3*, 1500324.
- (2) Wang, H.; Kim, D. H. Perovskite-based photodetectors: Materials and devices. *Chem. Soc. Rev.* **2017**, *46*, 5204–5236.
- (3) Cao, Y.; Wang, N.; Tian, H.; Guo, J.; Wei, Y.; Chen, H.; Miao, Y.; Zou, W.; Pan, K.; He, Y.; Cao, H.; Ke, Y.; Xu, M.; Wang, Y.; Yang, M.; Du, K.; Fu, Z.; Kong, D.; Dai, D.; Jin, Y.; Li, G.; Li, H.; Peng, Q.; Wang, J.; Huang, W. Perovskite light-emitting diodes based on spontaneously formed submicrometre-scale structures. *Nature* **2018**, *562*, 249–253.
- (4) Zhu, H.; Fu, Y.; Meng, F.; Wu, X.; Gong, Z.; Ding, Q.; Gustafsson, M. V.; Trinh, M. T.; Jin, S.; Zhu, X. Y. Lead halide perovskite nanowire lasers with low lasing thresholds and high quality factors. *Nat. Mater.* **2015**, *14*, 636.
- (5) Utzat, H.; Sun, W.; Kaplan, A. E. K.; Krieg, F.; Ginterseder, M.; Spokoiny, B.; Klein, N. D.; Shulenberger, K. E.; Perkinson, C. F.; Kovalenko, M. V.; Bawendi, M. G. Coherent single-photon emission from colloidal lead halide perovskite quantum dots. *Science* **2019**, *363*, 1068.
- (6) Protesescu, L.; Yakunin, S.; Bodnarchuk, M. I.; Krieg, F.; Caputo, R.; Hendon, C. H.; Yang, R. X.; Walsh, A.; Kovalenko, M. V. Nanocrystals of cesium lead halide perovskites (CsPbX<sub>3</sub>, X = Cl, Br, and I): Novel optoelectronic materials showing bright emission with wide color gamut. *Nano Lett.* **2015**, *15*, 3692–3696.
- (7) Nedelcu, G.; Protesescu, L.; Yakunin, S.; Bodnarchuk, M. I.; Grotevent, M. J.; Kovalenko, M. V. Fast anion-exchange in highly luminescent nanocrystals of cesium lead halide perovskites (CsPbX<sub>3</sub>, X = Cl, Br, I). *Nano Lett.* **2015**, *15*, 5635–5640.
- (8) Li, Y.-F.; Feng, J.; Sun, H.-B. Perovskite quantum dots for light-emitting devices. *Nanoscale* **2019**, *11*, 19119–19139.
- (9) Zhu, L.; Lai, Q.; Zhai, W.; Chen, B.; Wang, Z. L. Piezo-phototronic effect enhanced polarization-sensitive photodetectors based on cation-mixed organic–inorganic perovskite nanowires. *Mater. Today* **2020**, *37*, 56–63.
- (10) Rakita, Y.; Bar-Elli, O.; Meirzadeh, E.; Kaslasi, H.; Peleg, Y.; Hodes, G.; Lubomirsky, I.; Oron, D.; Ehre, D.; Cahen, D. Tetragonal CH<sub>3</sub>NH<sub>3</sub>PbI<sub>3</sub> is ferroelectric. *Proc. Natl. Acad. Sci. U. S. A.* **2017**, *114*, E5504–E5512.
- (11) Leppert, L.; Reyes-Lillo, S. E.; Neaton, J. B. Electric field- and strain-induced Rashba effect in hybrid halide perovskites. *J. Phys. Chem. Lett.* **2016**, *7*, 3683–3689.
- (12) Wang, Z. L. Nanopiezotronics. *Adv. Mater.* **2007**, *19*, 889–892.
- (13) Wang, Z. L. The new field of nanopiezotronics. *Mater. Today* **2007**, *10*, 20–28.
- (14) Wu, W.; Wang, L.; Li, Y.; Zhang, F.; Lin, L.; Niu, S.; Chenet, D.; Zhang, X.; Hao, Y.; Heinz, T. F.; Hone, J.; Wang, Z. L. Piezoelectricity of single-atomic-layer MoS<sub>2</sub> for energy conversion and piezotronics. *Nature* **2014**, *514*, 470–474.
- (15) Wu, W.; Wang, Z. L. Piezotronics and piezo-phototronics for adaptive electronics and optoelectronics. *Nat. Rev. Mater.* **2016**, *1*, 16031.

- (16) Wang, L.; Liu, S.; Feng, X.; Zhang, C.; Zhu, L.; Zhai, J.; Qin, Y.; Wang, Z. L. Flexoelectronics of centrosymmetric semiconductors. *Nat. Nanotechnol.* **2020**, *15*, 661–667.
- (17) Zhu, L.; Wang, Z. L. Recent progress in piezo-phototronic effect enhanced solar cells. *Adv. Funct. Mater.* **2019**, *29*, 1808214.
- (18) Zhu, L.; Wang, L.; Xue, F.; Chen, L.; Fu, J.; Feng, X.; Li, T.; Wang, Z. L. Piezo-phototronic effect enhanced flexible solar cells based on n-ZnO/p-SnS core-shell nanowire array. *Adv. Sci.* **2017**, *4*, 1600185.
- (19) Chen, M.; Pan, C.; Zhang, T.; Li, X.; Liang, R.; Wang, Z. L. Tuning light emission of a pressure-sensitive silicon/ZnO nanowires heterostructure matrix through piezo-phototronic effects. *ACS Nano* **2016**, *10*, 6074–6079.
- (20) Pan, C.; Dong, L.; Zhu, G.; Niu, S.; Yu, R.; Yang, Q.; Liu, Y.; Wang, Z. L. High-resolution electroluminescent imaging of pressure distribution using a piezoelectric nanowire LED array. *Nat. Photonics* **2013**, *7*, 752–758.
- (21) Lin, P.; Zhu, L.; Li, D.; Xu, L.; Pan, C.; Wang, Z. Piezo-phototronic effect for enhanced flexible MoS<sub>2</sub>/WSe<sub>2</sub> van der Waals photodiodes. *Adv. Funct. Mater.* **2018**, *28*, 1802849.
- (22) Lai, Q.; Zhu, L.; Pang, Y.; Xu, L.; Chen, J.; Ren, Z.; Luo, J.; Wang, L.; Chen, L.; Han, K.; Lin, P.; Li, D.; Lin, S.; Chen, B.; Pan, C.; Wang, Z. L. Piezo-phototronic effect enhanced photodetector based on CH<sub>3</sub>NH<sub>3</sub>PbI<sub>3</sub> single crystals. *ACS Nano* **2018**, *12*, 10501–10508.
- (23) Zhu, L.; Zhang, Y.; Lin, P.; Wang, Y.; Yang, L.; Chen, L.; Wang, L.; Chen, B.; Wang, Z. L. Piezotronic effect on Rashba spin-orbit coupling in a ZnO/P3HT nanowire array structure. *ACS Nano* **2018**, *12*, 1811–1820.
- (24) Zhu, L.; Wang, Z. L. Piezotronic effect on Rashba spin-orbit coupling based on MaPbI<sub>3</sub>/ZnO heterostructures. *Appl. Phys. Lett.* **2020**, *117*, 071601.
- (25) Sze, S. M.; Ng, K. K. *Physics of semiconductor devices*; Wiley: New York, 2006.
- (26) Li, J.; Gan, L.; Fang, Z.; He, H.; Ye, Z. Bright tail states in blue-emitting ultrasmall perovskite quantum dots. *J. Phys. Chem. Lett.* **2017**, *8*, 6002–6008.
- (27) Wright, A. D.; Milot, R. L.; Eperon, G. E.; Snaith, H. J.; Johnston, M. B.; Herz, L. M. Band-tail recombination in hybrid lead iodide perovskite. *Adv. Funct. Mater.* **2017**, *27*, 1700860.
- (28) Kim, T.-H.; Jun, S.; Cho, K.-S.; Choi, B. L.; Jang, E. Bright and stable quantum dots and their applications in full-color displays. *MRS Bull.* **2013**, *38*, 712–720.
- (29) Ye, S.; Xiao, F.; Pan, Y. X.; Ma, Y. Y.; Zhang, Q. Y. Phosphors in phosphor-converted white light-emitting diodes: Recent advances in materials, techniques and properties. *Mater. Sci. Eng., R* **2010**, *71*, 1–34.
- (30) Cohen, R. E. Origin of ferroelectricity in perovskite oxides. *Nature* **1992**, *358*, 136–138.
- (31) Lee, J.-H.; Jeong, Y. K.; Park, J. H.; Oak, M.-A.; Jang, H. M.; Son, J. Y.; Scott, J. F. Spin-canting-induced improper ferroelectricity and spontaneous magnetization reversal in SmFeO<sub>3</sub>. *Phys. Rev. Lett.* **2011**, *107*, 117201.
- (32) Li, X.; Chen, S.; Liu, P.-F.; Zhang, Y.; Chen, Y.; Wang, H.-L.; Yuan, H.; Feng, S. Evidence for ferroelectricity of all-inorganic perovskite CsPbBr<sub>3</sub> quantum dots. *J. Am. Chem. Soc.* **2020**, *142*, 3316–3320.
- (33) Kim, M.; Im, J.; Freeman, A. J.; Ihm, J.; Jin, H. Switchable  $S = 1/2$  and  $J = 1/2$  Rashba bands in ferroelectric halide perovskites. *Proc. Natl. Acad. Sci. U. S. A.* **2014**, *111*, 6900–6904.
- (34) Li, J.; Haney, P. M. Circular photogalvanic effect in organometal halide perovskite CH<sub>3</sub>NH<sub>3</sub>PbI<sub>3</sub>. *Appl. Phys. Lett.* **2016**, *109*, 193903.
- (35) Zheng, F.; Tan, L. Z.; Liu, S.; Rappe, A. M. Rashba spin-orbit coupling enhanced carrier lifetime in CH<sub>3</sub>NH<sub>3</sub>PbI<sub>3</sub>. *Nano Lett.* **2015**, *15*, 7794–7800.
- (36) Ganichev, S.; Prettl, W. Spin photocurrents in quantum wells. *J. Phys.: Condens. Matter* **2003**, *15*, R935.